Supporting Information

Boosting ammonia decomposition for hydrogen production over Co/CeO_2 catalysts via Sr doping

Linghui Su,[a] Fanke Zeng,[a] Jiajie Wang,[b] Qasim Qasim,[a] Xiaoli Liu, [c] Jing Li,[d] Hao Li *[e] and Wanglai Cen *[a]

[a] *Institute of New Energy and Low-Carbon Technology, Sichuan University, Chengdu 610065, China*

[b] *National Key Laboratory of Porous Materials for Gas Separation and Conversion, Southwest Institute of Chemical Co., Ltd., Chengdu 610225, China*

[c] *Sichuan Shunan Xingzhu Ecological Technology Co., Ltd., Yibin 644000, China*

[d] *College of Carbon Neutrality and Future Technology, Sichuan University, Chengdu 610065, China*

[e] *Advanced Institute for Materials Research (WPI-AIMR), Tohoku University, Sendai, Miyagi 980-8577, Japan*

** Corresponding author. E-mail: cenwanglai@scu.edu.cn. li.hao.b8@tohoku.ac.jp*

Experimental section

Materials

Cobalt (III) nitrate hexahydrate ($Co(NO_3)_3{\cdot}6H_2O$, 99%), cerium (III) nitrate hexahydrate ($Ce(NO_3)_3{\cdot}6H_2O$, 99%), strontium (II) nitrate hexahydrate ($Sr(NO_3)_2{\cdot}6H_2O$, 99%), lanthanum (III) nitrate hexahydrate ($La(NO_3)_3{\cdot}6H_2O$, 99%), barium (II) nitrate hexahydrate ($Ba(NO_3)_2{\cdot}6H_2O$, 99%), yttrium (II) nitrate hexahydrate ($Y(NO_3)_3{\cdot}6H_2O$, 99%), samarium (III) nitrate hexahydrate ($Sm(NO_3)_3{\cdot}6H_2O$, 99%), calcium (II) nitrate hexahydrate ($Ca(NO_3)_2{\cdot}6H_2O$, 99%), anhydrous citric acid and ethylene glycol were purchased from Sigma-Aldrich. All chemicals were used directly without further treatment.

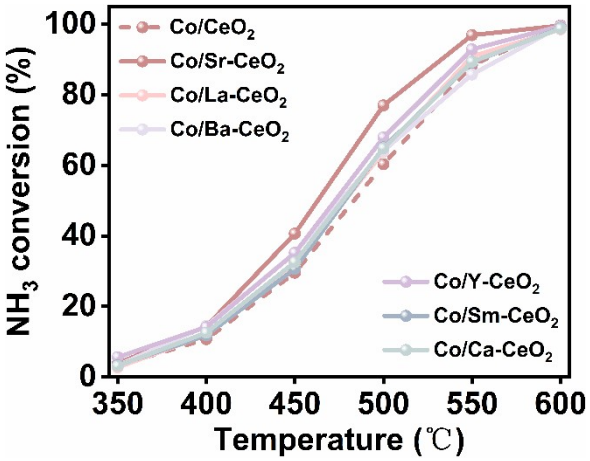

Figure S1. NH_3 decomposition conversion over the Co/CeO_2 catalyst with different promoters (Sr, La, Ba, Y, Sm and Ca).

The Co/CeO_2 catalysts doped with different promoters (Sr, La, Ba, Y, Sm and Ca) were prepared using the same method as that for $Co/Sr\text{-}CeO_2$, simply by replacing $Sr(NO_3)_2{\cdot}6H_2O$ with the corresponding metal nitrate.

Among the various promoters screened (Sr, La, Ba, Y, Sm, Ca), Sr exhibited the most pronounced promotional effect for ammonia decomposition. This superiority can be attributed to several interrelated factors. First, the ionic radius of Sr^{2+} (118 pm) is optimal for incorporation into the CeO_2 lattice-large enough to induce lattice strain and promote oxygen vacancy formation, yet small enough to avoid surface segregation. Second, Sr possesses moderate basicity, which provides sufficient electron-donating capability to enrich Co electron density without excessively stabilizing reaction intermediates.

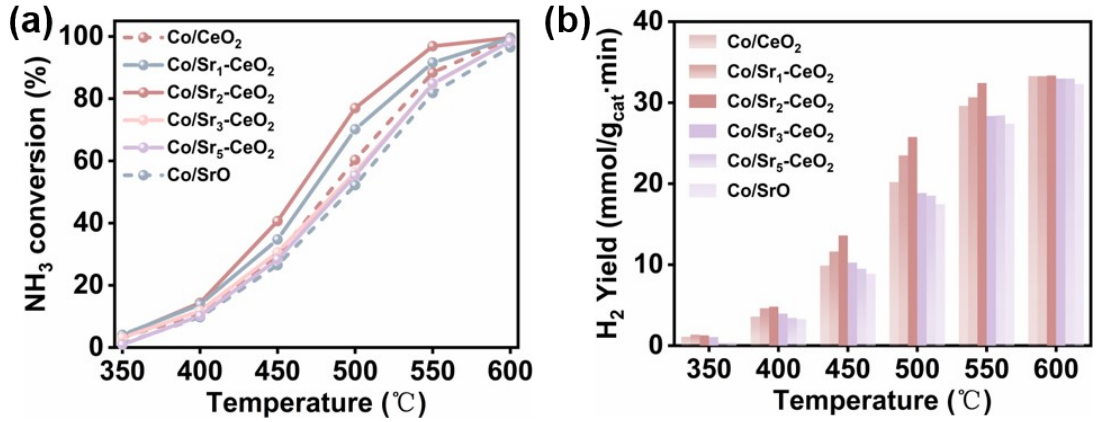

Figure S2. (a) NH_3 decomposition conversion and (b) H_2 yield in Co/Sr-CeO_2 catalyst with different Sr content.

The Co/Sr-CeO_2 catalysts with different Sr contents were synthesized following the same procedure as that for Co/Sr-CeO_2, with the only modification being the amount of $Sr(NO_3)_2{\cdot}6H_2O$ precursor used. Specifically, the Co/Sr_1-CeO_2, Co/Sr_2-CeO_2, Co/Sr_3-CeO_2, and Co/Sr_5-CeO_2 catalysts were prepared using 1, 2, 3, and 5 mmol of $Sr(NO_3)_2{\cdot}6H_2O$, respectively. The total amount of $Sr(NO_3)_2{\cdot}6H_2O$ and $Ce(NO_3)_3{\cdot}6H_2O$ was kept constant at 10 mmol in all samples.

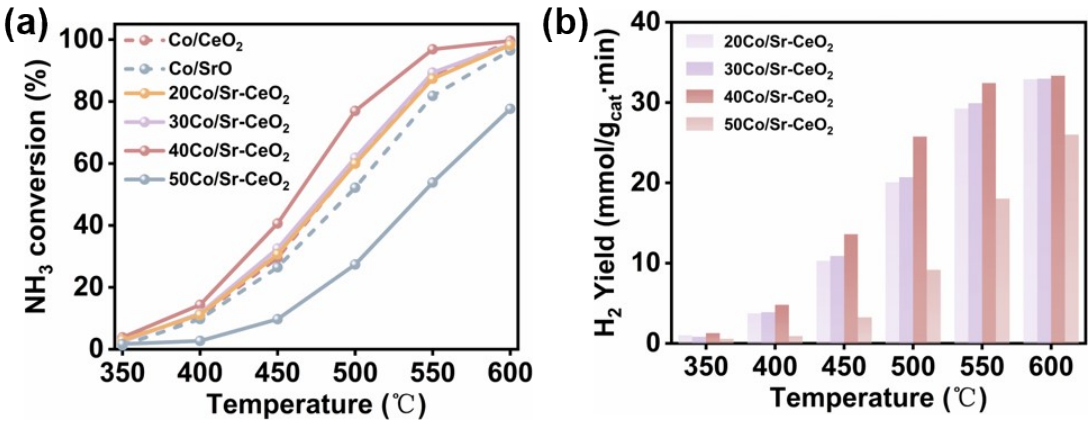

Figure S3. (a) NH_3 decomposition conversion and (b) H_2 yield in Co/Sr-CeO_2 catalyst with different Co content.

The Co/Sr-CeO_2 catalysts with different Co loadings were synthesized following the same procedure as that for Co/Sr-CeO_2, with the $Co(NO_3)_3{\cdot}6H_2O$ precursor amount being the only variable. Specifically, the 20Co/Sr-CeO_2, 30Co/Sr-CeO_2, 40Co/Sr-CeO_2, and 50Co/Sr-CeO_2 catalysts were prepared using 20, 30, 40, and 50 mmol of $Co(NO_3)_3{\cdot}6H_2O$, respectively.

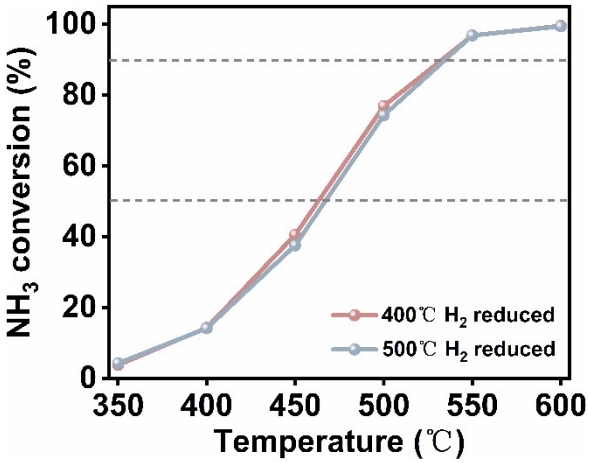

Figure S4. NH_3 decomposition conversion in Co/Sr-CeO_2 catalyst with different H_2 reduction temperature.

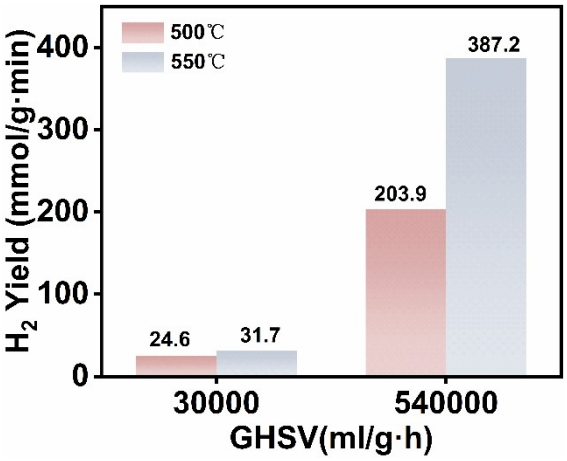

Figure S5. H_2 yield at different temperatures and GHSV over Co/Sr-CeO_2 catalyst.

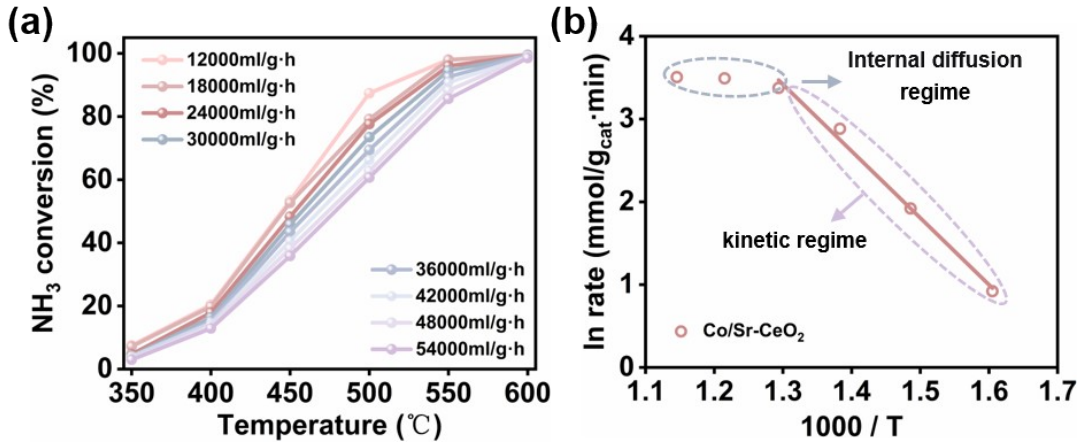

Figure S6. (a) NH_3 decomposition conversion with different GHSV over Co/Sr-CeO_2 catalyst. (b) The apparent activation energy (E_a) for Co/Sr-CeO_2 catalysts at GHSV = 12000 mL/g·h.

To assess the reliability of our kinetic data, we examined the temperature dependence of the reaction rate at the lowest GHSV tested (12000 ml/g·h). As shown in Fig. S6b, the Arrhenius plot exhibits excellent linearity from 350 to 500 ℃, indicating kinetically controlled behavior in this range. Above 500 ℃, downward curvature is observed, suggesting the onset of internal diffusion limitations at high temperatures under low space velocity. This interpretation is quantitatively confirmed by Weisz-Prater analysis, yielding C_{WP} = 0.082 at 500 °C. Therefore, all kinetic parameters reported in this study (including the E_a at GHSV = 30000 ml/g·h) are derived from the kinetically controlled regime (≤ 500 °C) and represent intrinsic catalytic properties.

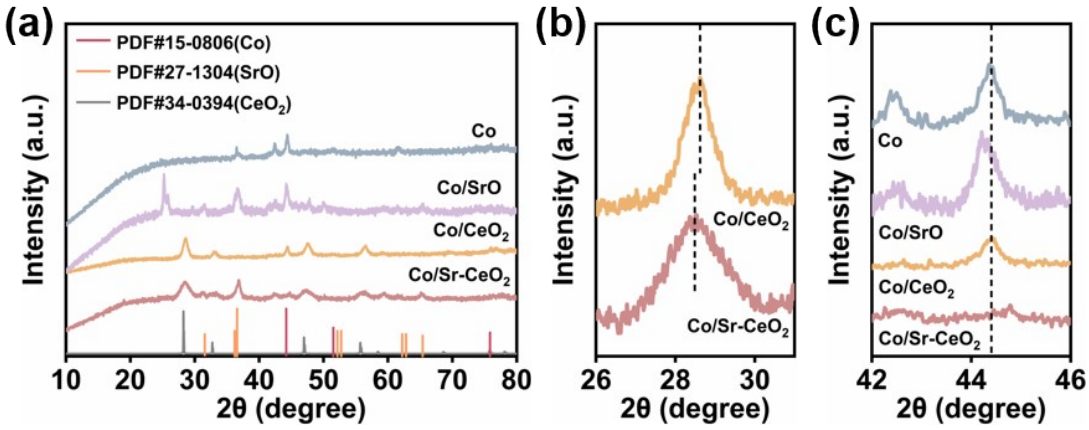

Figure S7. XRD patterns of Co/Sr-CeO_2, Co/CeO_2, Co/SrO and Co catalysts after H_2 reduction.

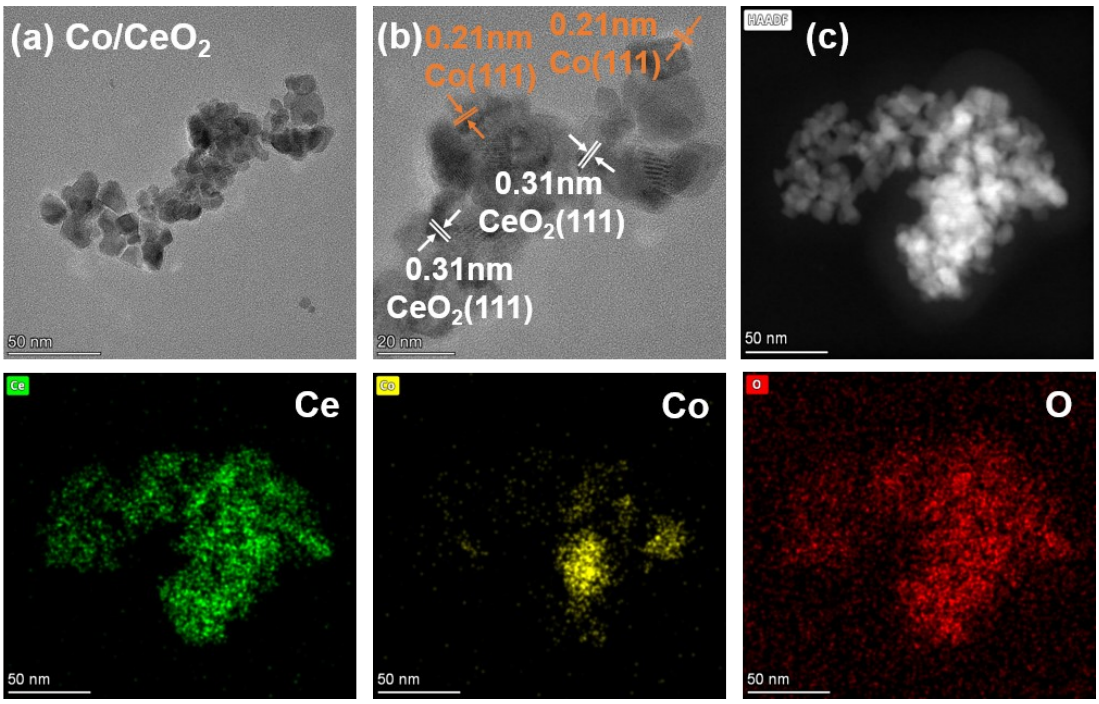

Figure S8. (a) TEM images, (b) HR-TEM images with marked lattice fringes of Co/Sr-CeO_2 catalyst. (c) The corresponding elemental mapping of Co/Sr-CeO_2 catalyst.

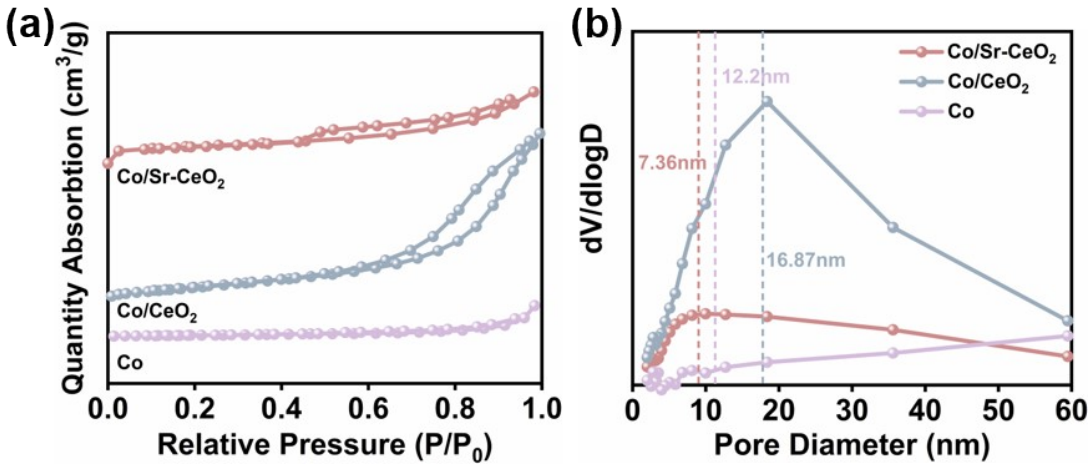

Figure S9. (a) N_2 adsorption-desorption isotherms, (b) BJH pore size distribution curves of Co/CeO_2, $Co/Sr\text{-}CeO_2$ and Co catalyst.

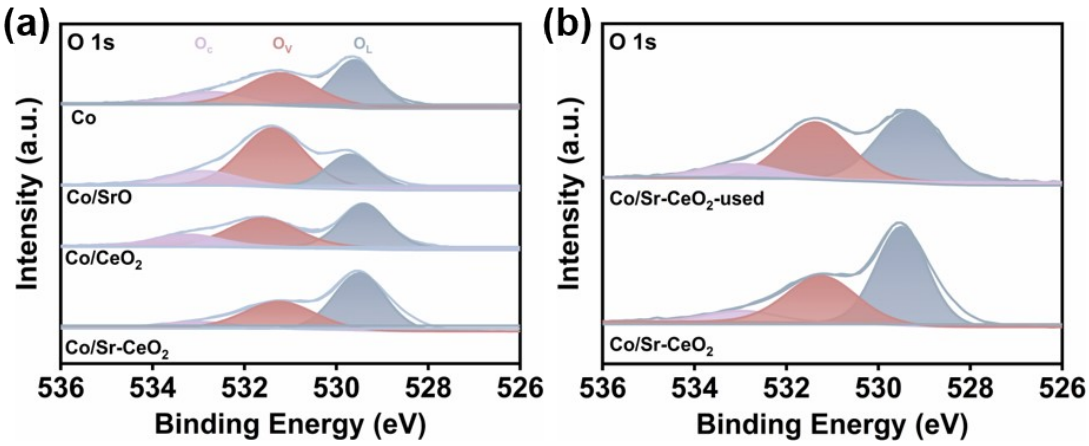

Figure S10. High-resolution Sr 3d XPS spectra of (a) Co/Sr-CeO_2, Co/CeO_2, Co/SrO and Co/Sr-CeO_2 catalysts and (b) used Co/Sr-CeO_2 catalysts.

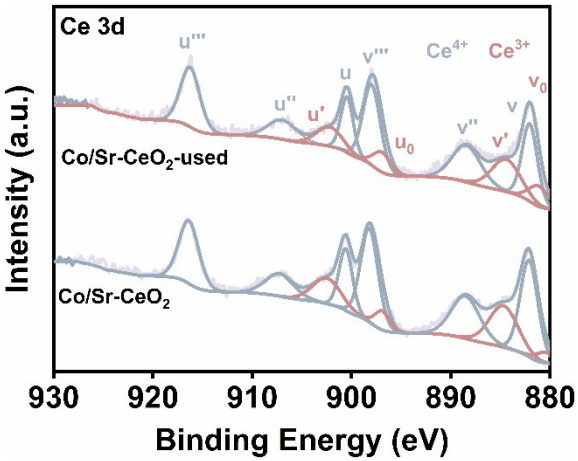

Figure S11. High-resolution Ce 3d XPS spectra of used Co/Sr-CeO_2 catalysts.

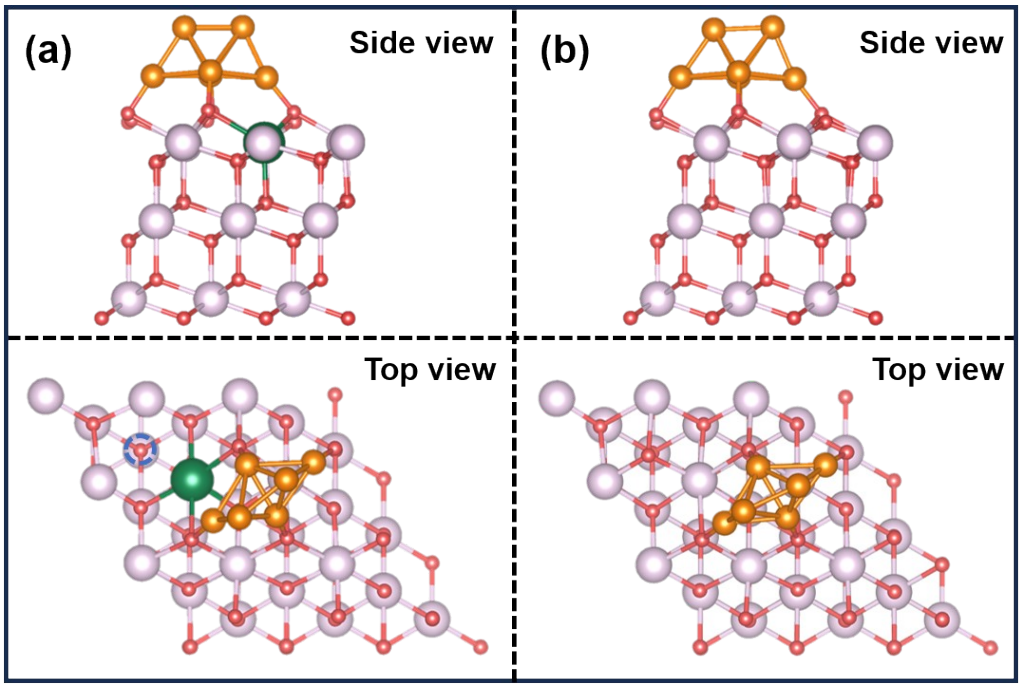

Figure S12. The DFT structure of (a) Co/Sr-CeO_2 and (b) Co/CeO_2 catalysts with side and top views. Blue circle represents oxygen vacancy (O_v).

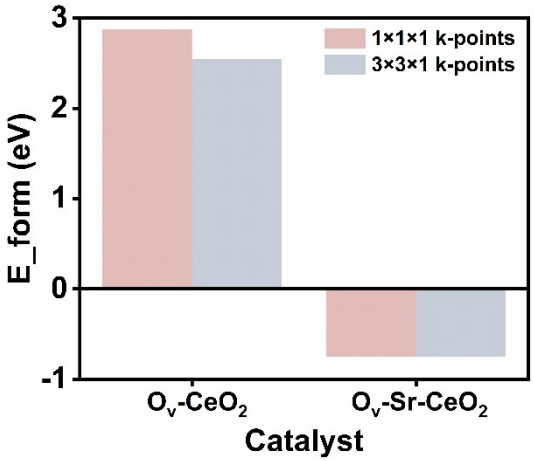

Figure S13. Comparison of formation energy of oxygen vacancy over CeO_2 and Sr-CeO_2 surface with different k-points.

A comparative test was conducted using 1×1×1 and 3×3×1 k-point meshes for calculating oxygen vacancy formation energies on CeO_2 and Sr-CeO_2 surfaces. While the absolute values exhibited minor variations between the two settings, the key comparative trends remained identical. This confirms that the computationally more efficient 1×1×1 k-point mesh is sufficient for reliably capturing the energetic trends, and was therefore adopted for all subsequent calculations.

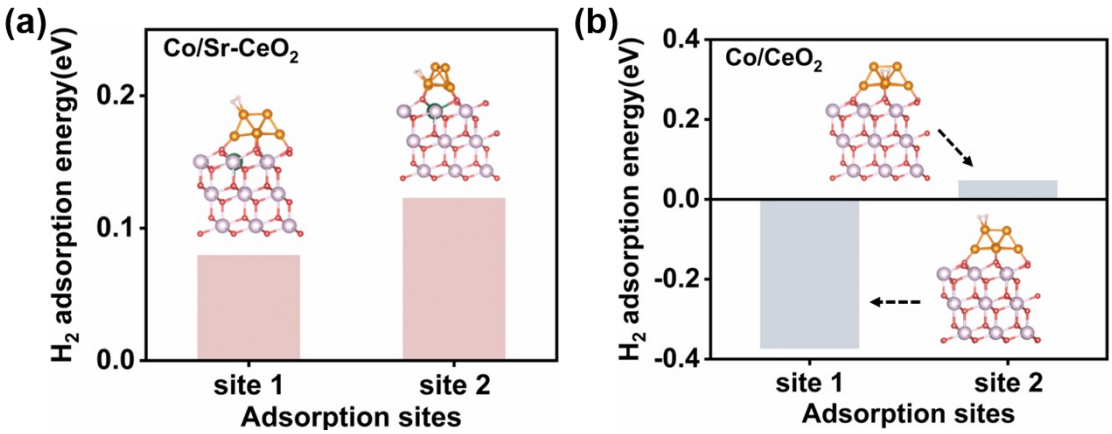

Figure S14. Comparison of H_2 adsorption energy and structure at different sites over (a) Co/Sr-CeO_2 and (b) Co/CeO_2 surfaces.

Table S1. Comparison of Co-based NH_3 decomposition catalyst reported recent years.

Catalyst	GHSV (ml/g·h)	Temperature (℃)	NH_3 conversion	H_2 production (mmol/g·min)	ref
Co/Sr-CeO_2	30000	500	76%	25.8	This work
		550	95%	32.4	
Co/La-Al_2O_3	9000	550	90%	8.9	1
Co-Ni/Y_2O_3	9000	550	85.02%		2
Co/$LaO_{1.5}$	12000	500	90.5%		3
Co/$YO_{1.5}$			75.6%		
$CoMoN_2$/CNTs	11000	600	71.5	8.8	4
Co/CeO_2-3DOM	6000	550	62%	4.2	5
FeCoNi/LaSrO-1.7	20000	550	75%		6
4Y_2O_3-Co/NC	20000	500	56.1%		7
Ba-Co/Y_2O_3	30000	500	87.5%	29.3	8
30%Co/SiC	30000	550	78.3%	25	9
$Co_9Ce_{0.5}Al_{0.5}O_x$	30000	500	65.3%		10
$LaCaCoTiO_{3-\delta}$	30000	700	63.9%	21.4	11

Table S2. The average crystallite size of the Co_3O_4 nanoparticles was estimated from the XRD patterns using the Scherrer equation.

	Co/Sr-CeO_2	Co/CeO_2	Co/SrO	Co
Average crystallite size (nm)	13.87	26.46	19.26	39.07

Table S3. The BET specific surface area, adsorption average pore diameter and pore volume of the prepared catalysts.

	Co/Sr-CeO_2	Co/CeO_2	Co
BET surface area(m^2/g)	16.10	23.86	3.243
Average pore diameter(nm)	7.36	12.2	16.87
Pore volume (cm^3/g)	0.0296	0.0728	0.0137

Table S4. The content of Ce^{3+} based on the Ce 3d XPS spectra.

	Co/Sr-CeO_2	Co/CeO_2	Co/Sr-CeO_2-used
Ce^{3+} / (Ce^{3+} + Ce^{4+})	26.35%	22.44%	27.59%

Reference

1 W. Wang, Y. Fu, W. Wang, M. Xiang, G. Chen, Y. Su and J. Duan, *Ceram. Int.*, 2024, **50**, 36604-36614.

2 H. Li, L. Guo, J. Qu, X. Fang, Y. Fu, J. Duan, W. Wang and C. Li, *Int. J. Hydrogen Energy*, 2023, **48**, 8985-8996.

3 H. Mizoguchi, S. Luo, M. Sasase, M. Kitano and H. Hosono, *J. Phys. Chem. Lett.*, 2025, **16**, 796–801.

4 Z. Zhao, H. Zou and W. Lin, *J. Rare Earths*, 2013, **31**, 247-250.

5 C. Huang, Y. Yu, X. Tang, Z. Liu, J. Zhang, C. Ye, Y. Ye and R. Zhang, *Appl. Surf. Sci.*, 2020, **532**, 147335.

6 Y. Li, K. Wang, Z. Wang, X. Wang, X. Chu, R. Zhang, S. Song, H. Zhang and X. Wang, *Adv. Energy Mater.*, 2025, 2405296-2405303.

7 Y. Zhu, H. Pan, Q. Li, X. Huang, W. Xi, H. Tang, W. Tu, S. Wang, H. Tang and H. Zhang, *Adv. Sci.*, 2024, **11**, 2406659.

8 K. Xu, Y.-Y. Zhang, W.-W. Wang, M. Peng, C. Ma, Y.-W. Zhang, C.-J. Jia, D. Ma and C.-H. Yan, *Angew. Chem., Int. Ed.*, 2025, **64**, e202416195.

9 R. Xu, F. Yin, J. Zhang, G. Li, G. Kofie, Y. Tan and B. Chen, *Catal. Today*, 2024, **437**, 114774.

10 K. Xu, N. Jiang, P. Wang, W.-W. Wang and C.-J. Jia, *Catal. Sci. Technol.*, 2024, **14**, 5678-5686.

11 H. Jeong, Y. H. Kim, W. Jang, Y. Ji, J.-E. Hong and J. Myung, *Solid State Ionics*, 2024, **416**, 116679.